# Resolving individual carrier dynamics with kHz single-shot optical-pump terahertz-probe spectroscopy in high magnetic fields

Blake S. Dastrup*[a], Peter R. Miedaner*[a], Zhuquan Zhang[a], Keith A. Nelson[a]
[a] Department of Chemistry, Massachusetts Institute of Technology, Cambridge MA, USA 02139
*Equal contribution

## ABSTRACT

We introduce a novel method of isolating carrier dynamics in optically excited semiconductors using optical-pump terahertz-probe spectroscopy, with a large external magnetic field to isolate different carrier types based on their cyclotron energies. We employ new echelon-based single-shot detection that utilizes a pair of 1D line array detectors which can read out at a 1 kHz repetition rate, reducing acquisition time by more than an order of magnitude. This enables collection of full 2D optical-pump/THz-probe scans at different magnetic fields. We demonstrate these capabilities by performing cyclotron resonance measurements in bulk silicon, and discover distinct carrier dynamics for electrons and holes, as well as their dependence on an external magnetic field.

**Keywords:** Terahertz, magnetic fields, Landau levels, carrier dynamics, semiconductor

## 1. INTRODUCTION

Terahertz time-domain spectroscopy (THz-TDS) has emerged as powerful tool to study charge [1-2], lattice [3], and spin [4-8] dynamics close to and far-from equilibrium on an ultrafast time scale. When combined with an external magnetic field, THz-TDS can be used to study emergent behavior. In particular, the quantization of charge-carrier motion by a uniform magnetic field into cyclotron resonances (CRs), known as the Landau quantization, has attracted a lot of interest due to their large electric dipoles and topological protection (Kohn's theorem) which lead to exotic physics such as the deep-strong coupling to a cavity vacuum field [9-11]. While THz-TDS is useful to study samples with an equilibrium carrier population, optical-pump terahertz-probe spectroscopy (OPTP) could help unravel carrier dynamics far from equilibrium. OPTP measurements are, however, hampered by the long acquisition times that would be required to resolve the full time-dynamics of an optically excited system. Since the conventional THz detection method, electro-optic (EO) sampling, is also a time-resolved measurement in which the THz electric field (E-field) is probed with an optical gate pulse in an EO crystal and the relative delay is scanned in a stepwise manner, an OPTP experiment requires that at least two separate time delays to be scanned to obtain a complete data set. This often requires days of acquisition times to achieve reasonable SNR, severely limiting the number of additional experimental parameters that can be explored.

Various methods to reduce data acquisition times have been proposed. One common technique involves replacing the optical delay line in a conventional EO sampling method with a stair-step echelon that produces temporally and spatially separated beamlets, which can then be imaged onto a camera such that each time step corresponds to a distinct set of pixels on the camera sensor [12-14]. Cameras are typically restricted to readout rates much lower than 1 kHz, which restricts echelon-based detection to lower repetition rates or requires use of specialized hardware to quickly readout small regions of a camera sensor. Another recent method relying on spectral encoding of temporal information has also been demonstrated at high repetition rates [15] but has limited time resolution $\delta t = 300$ fs meaning only frequencies up to ~1.5 THz can be resolved. Here we report a new echelon-based single-shot detection scheme for OPTP experiments in a magnetic field using 1D array detectors which allow for high-speed shot-to-shot balanced detection with high temporal resolution [16]. To test the capabilities of our setup, we measured the spectro-temporal evolution and B-field dependence of carrier CR in bulk high-resistivity Si following an 800 nm optical excitation pulse. While conventional OPTP measurements of carrier dynamics observe the combined response of all charge carriers, the collapse of free-carrier gases into distinct cyclotron resonances allows the evolution of individual carriers to be disentangled.

## 2. METHODS

The OPTP experimental setup (Fig. 1a) consists of three beam paths all derived from the 4 mJ, 100 fs output of a Ti:Sapphire regenerative amplifier with an 800 nm center wavelength. The THz generation beam (2 mJ) is directed onto

Real-time Measurements, Rogue Phenomena, and Single-Shot Applications IX, edited by
Daniel R. Solli, Georg Herink, Serge Bielawski, Proc. of SPIE Vol. 12870, 1287005

a 1 mm thick zinc telluride (ZnTe) crystal. The resulting THz beam propagates into the Ø 100 mm bore of a superconducting solenoid magnet (0-9 T) parallel to the applied magnetic field, $\boldsymbol{B}_{\mathbf{ext}}$, and is focused to a spot size of ~1 mm by 1-inch paraboloid mirrors positioned at the center of the B-field (Fig 1b.), and is collected by an identical paraboloid and directed out of the magnetic bore. The 1.6 mJ optical pump beam is vertically displaced from the THz generating beam and is directed into the bore parallel to the THz generating beam. The collimated beam is directed onto the sample with a spot size of ~3 mm with an incidence angle of approximately 46° and is delayed using an optical delay-line (Fig. 1b). The EO sampling gate beam is reflected from a stairstep echelon, creating a sequence of 500 pulses with an interpulse delay of ~40 fs, which corresponds to an overall time window of ~20 ps. The beam at the echelon plane is relayed through a 4f imaging system (L5:L6, and then focused and recombined with the THz beam using a pellicle beamsplitter (PBS) onto the EO detection crystal (ZnTe). After the crystal, the gate beam is recollimated and relayed to the detectors through a pair of 4f imaging systems. Inserted into the beam path are a quarter waveplate, which serves to balance the intensity of the gate beam into any set of orthogonal polarizations, and a Wollaston prism, which separates the gate beam into two orthogonal polarizations. The two polarization components are parallelized and focused by a compound cylindrical lens (a pair of two separated cylindrical lenses, shown in Fig. 1c) onto a pair of parallel 1D detector arrays (Synertronic Glaz LineScan-I-Gen2) with 12 mm spacing, which are read out at a 1 kHz frame rate to achieve shot-to-shot balancing. We utilize the calibration procedure proposed by Gao [12] to map pixels to time-delays.

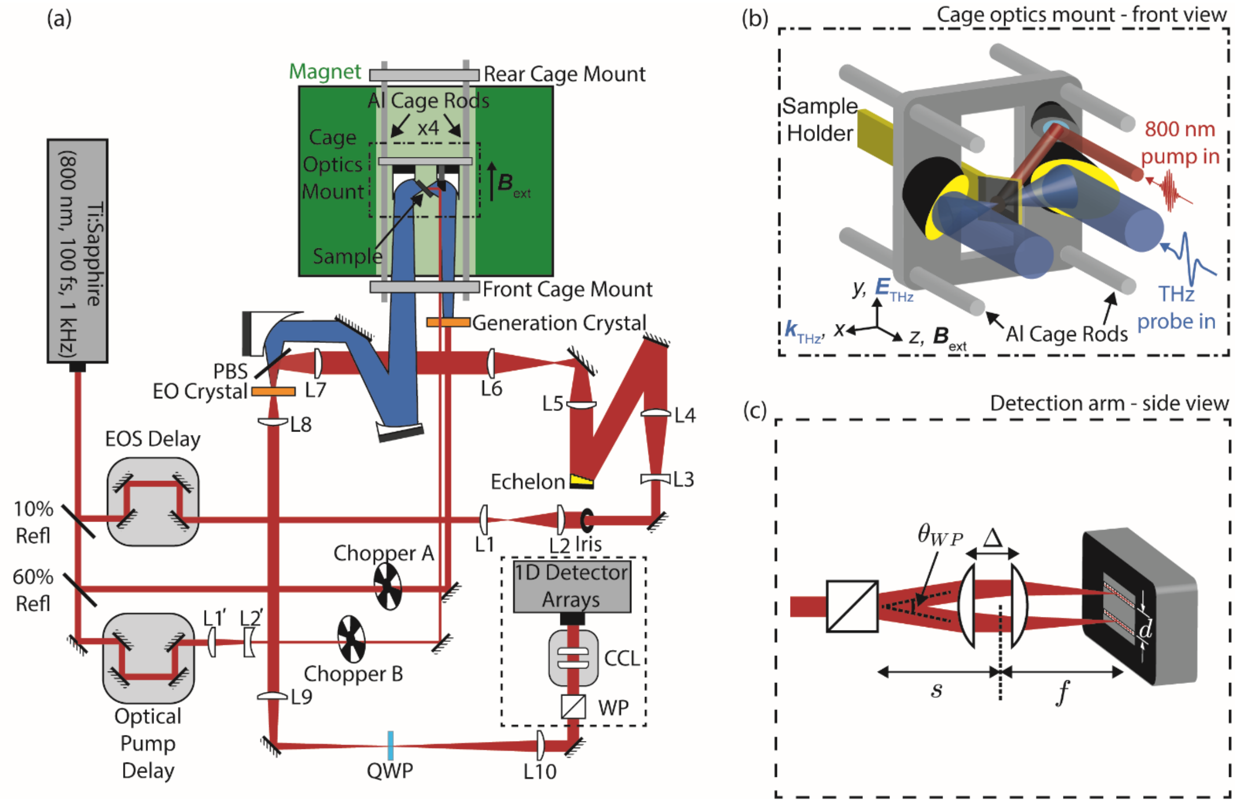

**Figure 1.** Single-shot high B-field OPTP optical setup. (a) Schematic of experimental setup. $\boldsymbol{B}_{\text{ext}}$: external B-field; BS: beam-splitter; $\boldsymbol{k}_{\text{THz}}$: THz propagation direction; $\boldsymbol{E}_{\text{THz}}$: THz E-field polarization direction; HWP: half waveplate; QWP: quarter waveplate; WP: Wollaston prism; CCL: compound cylindrical lens; L1-L4, probe beam expanding telescopes (1:3); L5-10, three successive 4f imaging systems ($f$ = 10, 10, 10, 5, 30, 30 cm); L1' ($f$ = 20 cm); L2' ($f$ = -7.5 cm); PBS: pellicle beam-splitter. (b) Front view of in-bore cage optics mount. THz beam path shown in blue. Optical pump path shown in red. Sample mount with 45° tilt depicted in gold. (c) Side view of probe beam path through Wollaston prism and compound cylindrical lens which focuses the two probe arms onto the two 1D array detectors.

We employ a differential chopping data collection scheme using two choppers that are inserted into the two pump beam paths and triggered using the 1 kHz trigger obtained from the laser. Labeling the THz generation beam as "A" and the optical pump as "B", chopper A runs at 500 Hz blocking every other pulse, while chopper B runs at 250 Hz blocking every other set of two pulses. Together, the two choppers produce each of the four combinations $A_{on}/B_{on}$, $A_{on}/B_{off}$, $A_{off}/B_{on}$, and $A_{off}/B_{off}$ over the course of 4 consecutive laser shots. We can thereby obtain the THz probe waveform (A), optical pump reference (B), the THz-probe waveform with optical pumping (AB), and the differential signal as follows,

$$\frac{\Delta I_\alpha}{I} = \frac{I_\alpha^+}{2I_0^+} - \frac{I_\alpha^-}{2I_0^-} = \frac{I_\alpha^+ - I_\alpha^-}{I_0} \tag{1}$$

$$\frac{\Delta I_{\text{diff}}}{I} = \frac{\Delta I_{\text{AB}}}{I} - \frac{\Delta I_{\text{A}}}{I} - \frac{\Delta I_{\text{B}}}{I} \tag{2}$$

where $I_\alpha^+$ and $I_\alpha^-$ are the raw 1D gate arrays for the two polarization arms of the balanced detection scheme ($\alpha = \{A, B, AB\}$), and $I_0^+$ and $I_0^-$ are the reference 1D gate arrays obtained when both pump beams are blocked by their respective choppers. The final equality in Eq (1) is true only when $I_0^+ = I_0^- = I_0/2$, which implies perfect balancing. We observe slight deviations (no larger than ~5%) in balancing from pixel to pixel, which we estimate leads to uncertainties in THz field amplitudes of ~0.5%.

THz transmission measurements were done in the Voigt geometry ($\boldsymbol{k}_{\text{THz}} \perp \boldsymbol{B}_{\text{ext}}$). A [100] undoped high-resistivity Si sample with 0.5 mm at 5 K. To probe different regions of k-space, the sample was oriented with the [100] axis either at 90° or 45° with respect to $\boldsymbol{B}_{\text{ext}}$ (where the angle is a rotation in the [011] plane of the sample). The 800 nm optical pump was set to a pulse energy of ~7 μJ, with corresponding fluences of 70 μJ/cm$^2$ for the 90° orientation, and 50 μJ/cm$^2$ for the 45° orientation.

## 3. RESULTS AND DISCUSSION

Figures 4a,c shows plots of the THz absorption spectrum as a function of optical-pump/THz-probe delay at different B-fields and for different sample orientations. The absorption spectrum, $A(\Omega)$, was calculated as

$$A(\Omega) = -\log\left(\frac{\Delta I_{AB}/I}{\Delta I_A/I}\right). \tag{2}$$

In the absence of a magnetic field, we observe a zero-frequency Drude response as expected in the free carrier gas approximation. Under a nonzero magnetic field, we observe the emergence of four Lorentzian peaks, all of which experience a blue shift with increasing magnetic field, as expected for CRs in the linear response regime. We attribute these four resonances to the CR response of heavy and light electron and holes that arise due to band degeneracy at the conduction band minimum and valence band maximum. The absorption features are fit to Lorentzians to extract the cyclotron frequencies, $\omega_c$. As shown in Fig. 2b,d, the frequencies follow a linear relationship with magnetic field, which is consistent with the Landau theory of charge carriers in a semiconductor $\omega_c = eB/m^*$, where the frequency is renormalized by an "effective mass," $m^*$, related to the band curvature [17]. Linear fits allow us to accurately extract effective masses for the four carrier types present in the spectra. For the 90° orientation we observe effective masses of $m^* = \{0.19 \pm 0.02, 0.244 \pm 0.002, 0.42 \pm 0.03, 0.64 \pm 0.03\}\, m_e$ and masses of $m^* = \{0.19 \pm 0.003, 0.26 \pm 0.003, 0.30 \pm 0.005, 0.50 \pm 0.02\}\, m_e$ for the 45° orientation, where $m_e$ is the mass of the electron. These masses are in good agreement with literature values [17]. Since orbital motion is restricted to a plane perpendicular to the external magnetic field, when the sample orientation is changed, the path in *k*-space traversed by the carriers is altered, leading to orientation-dependent effective masses, as confirmed by the drastic change in response when the sample surface normal is 90° and 45° from the external magnetic field.

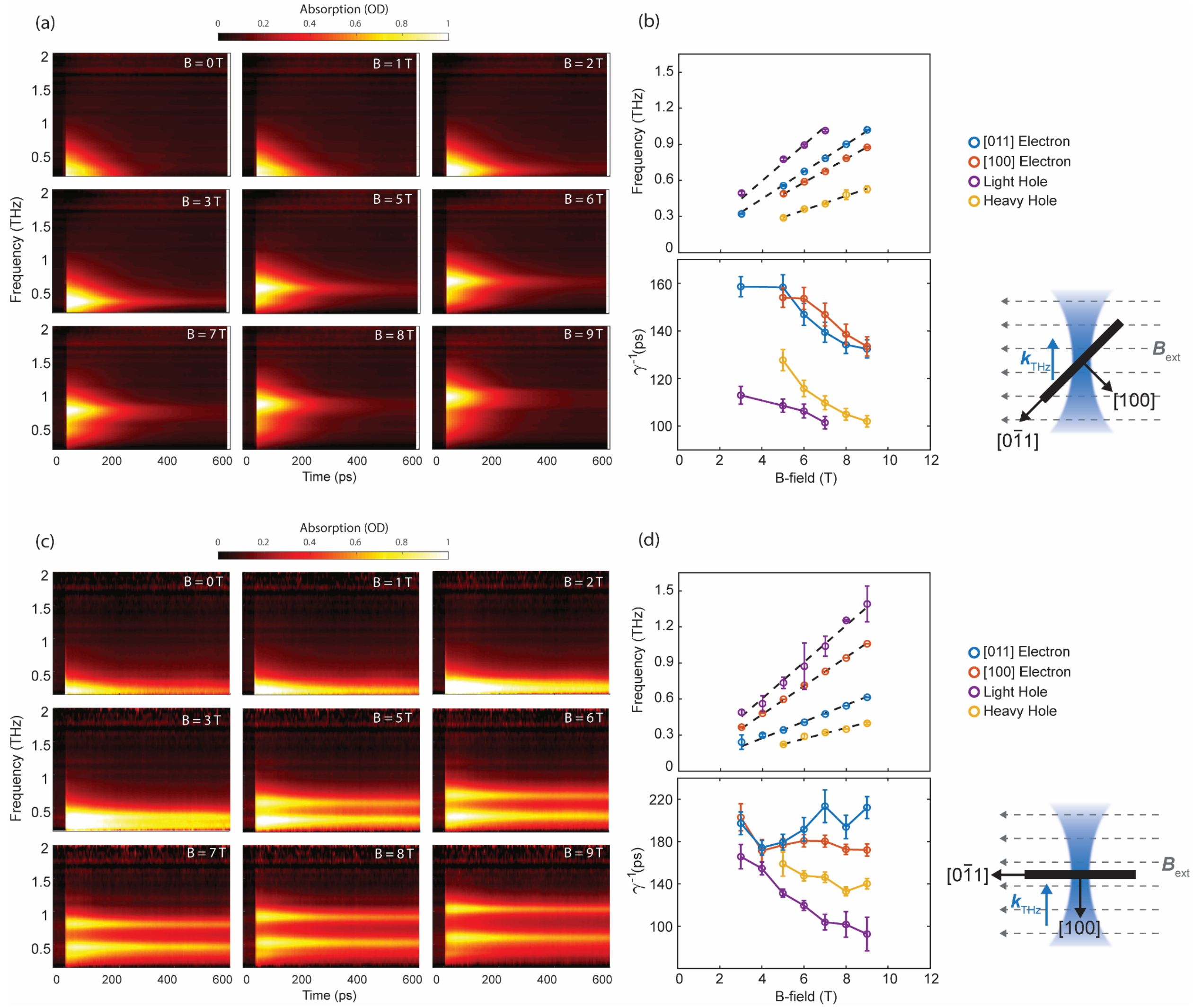

**Figure 2.** Cyclotron resonance spectra from [100] high-resistivity silicon. THz absorption as a function of optical pump/THz time delay plotted for $|\boldsymbol{B}_{\text{ext}}| = 0\text{-}9$ T and samples oriented at (a) 45° and (c) 90° with respect to $\boldsymbol{B}_{\text{ext}}$ as depicted by the diagrams on the right hand side of the figure. (b),(d) CR center frequencies (top) and inverse decay constant (bottom) as a function of external B-field. Error bars are the 95% confidence intervals extracted from (top) Lorentzian fits of the resonances and (bottom) exponential fits of the decay curves. The relationship between CR frequency and carrier effective mass is given by $\omega_c = eB/m^*$, where $e$ is the electron charge, and $m^*$ is the effective mass. We see four distinct resonances at both 45° and 90° sample orientation. Carrier relaxation is resolved into the four carrier types and we see distinct decay times for each carrier as well as a general trend of decreasing carrier lifetime with increasing B-field, with some exceptions.

Importantly, we are able to apply the above analysis as a function of OPTP time-delay to monitor the dynamics of individual carriers. At each time delay, the amplitude of the Lorentzian fit is proportional to the carrier density. It should be noted that the intensity of these peaks depends on the mobility of the carriers, and thus carriers which have relaxed to trapped states will not contribute to the signal. The signal amplitudes can then be fit to a single exponential function $f(\tau) = \exp(-\gamma\tau)$, where $\gamma$ is the decay rate constant, which are shown as a function of magnetic field in Figs 4b,d. The decay dynamics are drastically shorter than those observed in previous OPTP studies of silicon at room temperature [15], which has been previously explained by Suzuki and Shimano as the slow formation of excitons at cryogenic temperatures [18]. Additionally, we observe that the electrons decay more slowly than the holes for both the 45° and 90° sample orientations. We also observe that all four of the carrier types exhibit B-field-dependent decay times. For the 45° sample orientation, the decay time constant for all four resonances decreases nearly monotonically with increasing B-field. For the 90° sample orientation, we also see clear differences among decay time constants for the different carrier types as well as B-field dependence. In this case, the decay time of the hole resonances decreases with increasing B-field, while that of the [011] electron is relatively flat, and the decay time of the [100] electron appears to increase with increasing B-field. B-field dependence of carrier relaxation has previously been observed in graphene [19,20], where it was argued that the nonuniform spacing of Landau levels in the presence of a B-field gave rise to a decrease in Auger scattering events, and thereby an increased carrier lifetime. Here we generally observe the opposite trend (relaxation rate increases with increasing B-field). However, Landau level splitting in bulk Si is essentially harmonic, giving rise to states are symmetrically distributed about the carrier energy. Furthermore, Landau level degeneracy increases with increasing B-field [21], which leads to an increased density of states in the vicinity of the carrier energy. These two effects together make it likely that the changes in level spacing and degeneracy alter the available scattering pathways as the magnetic field increases, which, in turn, leads to an observable increase in the decay rate of excited carriers.

## 4. CONCLUSION

Our experimental setup permits OPTP spectroscopy in an external magnetic field with single-shot readout at high repetition rates. The SNR ratio obtained with economical 1D array detectors is on par with what has been recently demonstrated for 2D THz spectroscopy based on high-speed cameras, allowing for the collection of full 2D optical-pump/THz-probe scans at different magnetic fields, effectively a 3D measurement, in a dramatically reduced amount of time compared to conventional EO sampling of the THz probe. The present cyclotron resonance measurements of photoexcited carriers in silicon have yielded magnetic field-dependent electron and hole effective masses and decay rates that are distinct among the different carrier types. A promising future direction is to strongly couple these CR modes with a cavity and to observe the change in relaxation and dissipation as a result of the formation of light-matter hybrids.

## ACKNOWLEDGEMENTS

This work was supported by the U.S. Department of Energy, Office of Basic Energy Sciences, under Award No. DE-SC0019126

## REFERENCES

[1] Ulbricht, R., Hendry, E., Shan, J., Heinz, T. F. & Bonn, M. Erratum: “Carrier dynamics in semiconductors studied with time-resolved terahertz spectroscopy.” *Rev. Mod. Phys.* 89, 029901 (2017). https://doi.org/10.1103/RevModPhys.89.029901

[2] Lan, Y., Tao, X., Kong, X., He, Y., Zheng, X., Sutton, M., Kanatzidis, M.G., Guo, H., Cooke, D.G. “Coherent charge-phonon correlations and exciton dynamics in orthorhombic CH3NH3PbI3 measured by ultrafast multi-THz spectroscopy.” *J. Chem. Phys*. 151, 214201 (2019). https://doi.org/10.1063/1.5127992

[3] Porer, M., Leierseder, U., Menard, J.-M., Dachraoui, H., Mouchliadis, L., Perakis, I.E., Heinzmann, U., Demsar, J., Rossnagel, K., Huber, R. “Non-thermal separation of electronic and structural orders in a persisting charge density wave.” *Nat. Mater.* 13, 857–861 (2014). https://doi.org/10.1038/nmat4042

[4] Li, X., Bamba, M., Yuan, N., Zhang, Q., Zhao, Y., Xiang, M., Xu, K., Jin, Z., Ren, W., Ma, G. *et. al.* “Observation of Dicke cooperativity in magnetic interactions.” *Science* 361, 794–797 (2018). https://doi.org/10.1126/science.aat5162

[5] Makihara, T., Hayashida, K., Noe, G.T., Li, X., Peraca, N.M., Ma, X., Jin, Z., Ren, W., Ma, G., Katayama, I, *et. al.* “Ultrastrong magnon–magnon coupling dominated by antiresonant interactions.” *Nat. Commun.* 12, 3115 (2021). https://doi.org/10.1038/s41467-021-23159-z

[6] Belvin, C. A., Baldini, E., Ozel, I.O., Mao, D., Po, H.C., Allington, C.J., Son, S., Kim, B.H, Kim, J., Hwang, I., *et. al.* “Exciton-driven antiferromagnetic metal in a correlated van der Waals insulator.” *Nat. Commun.* 12, 4837 (2021). https://doi.org/10.1038/s41467-021-25164-8

[7] Zhang, Z., Gao, F.Y., Chien, Y.C., Liu, Z.J., Curtis, J.B., Sung, E.R., Ma, X., Ren, W., Cao, S., Narang, P., Hoegen, A.V., Baldini, E., Nelson, K.A. “ Terahertz-field-driven magnon upconversion in an antiferromagnet.” *Nat. Phys*. (2024) https://doi.org/10.1038/s41567-023-02350-7

[8] Zhang, Z., Gao, F.Y., Curtis, J.B., Liu, Z.J., Chien, Y.C., Hoegen, A.V., Wong, M.T., Kurihara, T., Suemoto, T., Narang, P., Baldini, E., Nelson, K.A. "Terahertz field-induced nonlinear coupling of two magnon modes in an antiferromagnet." *Nat. Phys*. https://doi.org/10.1038/s41567-024-02386-3

[9] Zhang, Q., Lou, M., Li, X., Reno, J.L., Pan, W., Watson, J.D., Manfra, M.J., Kono, J. "Collective non-perturbative coupling of 2D electrons with high-quality factor terahertz cavity photons." *Nat. Phys.* (2016) https://doi.org/10.1038/nphys3850

[10] Rokaj, V., Wang, J., Sous, J., Penz, M., Ruggenthaler, M., Rubio, A. "Weakened topological protection of the quantum hall effect in a cavity." *Phys. Rev. Let.* 131, 196602 (2023) https://doi.org/10.1103/PhysRevLett.131.196602

[11] Bayer, A., Pozimski, M., Schambeck, S., Schuh, D., Huber, R., Bougeard, D., Lange, C. "Terahertz light-matter interaction beyond unity coupling strength." *Nano Lett.* 17, 10, 6340-6344 (2017) https://doi.org/10.1021/acs.nanolett.7b03103

[12] Gao, F. Y., Zhang, Z., Liu, Z.-J., Nelson, K. A. "High-speed two-dimensional terahertz spectroscopy with echelon-based shot-to-shot balanced detection." *Opt. Lett.* 47, 3479–3482 (2022). https://doi.org/10.1364/OL.462624

[13] Mead, G., Katayama, I., Takeda, J., Blake, G. A. "An echelon-based single shot optical and terahertz Kerr effect spectrometer." *Rev. Sci. Instrum.* 90, 053107 (2019). https://doi.org/10.1063/1.5088377

[14] Noe, G. T., Katayama, I., Katsutani, F., Allred, J., Horowitz, J.A., Sullivan, D.M., Zhang, Q., Sekiguchi, F., Woods, G.L., Hoffmann, M.C., *et. al.* "Single-shot terahertz time-domain spectroscopy in pulsed high magnetic fields." *Opt. Express* 24, 30328–30337 (2016). https://doi.org/10.1364/OE.24.030328

[15] Couture, N., Cui, W., Lippl, M., Ostic, R., Fandio, D.J.J., Yalavarthi, E.K., Vishnuradhan, A., Gamouras, A., Joly, N.Y., Menard, J.-M. "Single-pulse terahertz spectroscopy monitoring sub-millisecond time dynamics at a rate of 50 kHz." *Nat. Comm.* 14, 2595 (2023). https://doi.org/10.1038/s41467-023-38354-3

[16] Dastrup, B.S., Miedaner, P.R., Zhang, Z., Nelson, K.A. "Optical-pump terahertz-probe spectroscopy in high magnetic fields with kHz single-shot detection." ." *ArXiv Prepr*. https://doi.org/10.48550/arXiv.2309.17393

[17] Dresselhaus, G., Kip, A., Kittel, C. "Cyclotron resonance of electrons and holes in silicon and germanium crystals." *Phys. Rev.* 98, 368 (1955). https://doi.org/10.1103/PhysRev.98.368

[18] Suzuki, T., Shimano, R.. "Time-resolved formation of excitons and electron-hold droplets in Si studied using terhaertz spectroscopy." *Phys. Rev. Let.* 103, 057401 (2009). https://doi.org/10.1103/PhysRevLett.103.057401

[19] Plochocka, P., Kossacki, P., Golnik, A., Kazimierczuk, T., Berger, C., de Heer, W.A., Potemski, M. "Slowing hot-carrier relaxation in graphene using a magnetic field." *Phys Rev B* 80, 245415 (2009). https://doi.org/10.1103/PhysRevB.80.245415

[20] But, D. B., Mittendorff, M., Consejo, C., Teppe, F., Mikhailov, N.N., Dvoretskii, S.A., Faugeras, C., Winnerl, S., Helm, M., Knap, W., *et. al*. "Suppressed Auger scattering and tunable light emission of Landau-quantized massless Kane electrons." *Nat. Photonics* 13, 783–787 (2019). https://doi.org/10.1038/s41566-019-0496-1

[21] Tong, D. "The quantum Hall effect: TIFR infosys lectures." *ArXiv Prepr. ArXiv160606687* (2016). https://doi.org/10.48550/arXiv.1606.06687